Differences in violin sounds caused by changes on arching profiles

Jesús A. Torres

Laboratorio de Acústica, Escuela de Laudería, Instituto Nacional de Bellas Artes y Literatura, Hidalgo #20 Centro, Querétaro, Qro., 76000, México.
e-mail: jesusalejandrott@yahoo.com.mx

Received 18 October 2023; accepted 5 February 2024

An experimentally calibrated numerical model was employed to examine the vibroacoustic impact of the arching profile in a violin soundbox, a study unattainable through experimental means alone. The finite element method successfully modeled the soundbox using the material properties of an actual violin, albeit with a simplified representation of the coupling with the air in the cavity and the forces from the strings. Achieving agreement with the real counterpart necessitated careful adjustment of the modal damping in the simulation. Damped models of violins are infrequently encountered. The impulse response of the soundbox model was obtained through the calculation of thousands of substeps induced by forced vibration. To streamline the time-domain analysis, the superimposed method was implemented instead of the more commonly used full option, resulting in a significant reduction in computational time. Additionally, synthetic musical notes, accounting for how the force of the strings is transmitted through the bridge, were employed as input to the soundbox model. Subsequently, the impulse responses were convolved with the synthetic notes to generate sounds. Through these procedures, the violin's performance was assessed as the height of the arching profile of the plates was adjusted. The results demonstrated that higher arching profiles led to a general increase in the resonant frequencies of the violin, perceptible in the sound generated by the model.

Keywords: Violin; Stradivari; finite element; ansys; signature modes.

DOI: https://doi.org/10.31349/RevMexFis.70.031002

1. Introduction

When analyzing vibratory systems, the considerable computational capacity of modern computers provides a robust option for simulating behaviors that are challenging to study through experiments alone. Nevertheless, implementing procedures for this purpose can often be intricate, sometimes requiring a combination of numerical methods with different natures. In the realm of musical instrument acoustics, there are instances of research employing various simulations working collaboratively to analyze the vibrational behavior of plucked and bowed instruments (*e.g.*, [1–3]). However, such research endeavors remain relatively scarce, limiting the depth of studies on violin design.

While the physical shape of the violin has been established for over 300 years, there remains a lack of clarity regarding the individual contributions of its components to its sound. The influence of the arching profile, in particular, poses a challenging subject for study, with limited objective data available on its impact on sound. In contrast to experimental investigations into components such as the bassbar [4], soundpost [5], or plate thickness [6], the arching profile cannot be easily modified once the instrument is completed. Furthermore, the use of wood in traditional violins prevents the creation of identical instruments with only the arching profile changed, even if pieces extracted from the same wooden blanks are employed, as seen in [7]. Such limitations can be overcome through computational simulations, where the vibroacoustic behavior of an adjustable violin can be calculated. The present paper aims to create such a simulation to analyze the influence of the arching profile.

Modeling the force required to drive a violin to produce realistic sounds is a highly complex task. Woodhouse and Galluzzo [8] outlined at least five crucial factors that must be considered: material properties of the strings, torsional motion, dimensions of the bow, coupling motions, and the role of rosin. Additionally, Guettler [9] elucidated the onset transient necessary to initiate Helmholtz motion on the bowed string. However, for the purpose of comparing the performance of various arching profiles in a model, simplifying these procedures may be sufficient to generate useful sounds.

On the other hand, when modeling the intricate vibratory behavior of a structure as complex as the violin, it is challenging to find a more versatile numerical technique than the Finite Element (FE) Method. For instance, Gough [10] employed this technique to create a mesh for a simplified violin model, establishing a connection between the arching height of free plates and their frequencies. However, the impact of altering the arching on the instrument's sound remained unexplored. More recently, Torres *et al*. [11] utilized a parametric FE model to investigate the vibratory effects of modifying various violin components, although the arching profile remained unchanged throughout the entire process. The present study employs an updated version of this parametric model.

Among the procedures necessary for this study, generating sound from numerical models of a violin is a relatively underexplored topic in the literature, as noted in Ref. [12]. They utilized real input forces measured on the violin bridge, which were filtered by admittances. The resulting time-domain files were then played to generate sound. This approach circumvents the complex calculations associated with modeling the propagation of sound waves through the air

TABLE I. Properties used in the materials of the finite element simulation. Bold values were measured from the real wooden blanks to make the Titian replica, while the rest of the properties were taken from [11]. Density units are given in kg/m^3 and shear and elastic modulus in GPa. The last column is the long-grain radiation ratio.

specie	ρ	E_L	E_T	G_{LT}	E_R	G_{LR}	G_{TR}	ν_{LT}	ν_{LR}	ν_{TR}	$R_L = \sqrt{E_L/\rho^3}$
spruce	**397**	**11.4**	**0.86**	**0.52**	1.2	0.988	.082	0.42	0.019	.03	13.4
maple	**587**	**13**	**2.5**	**2.25**	0.937	0.656	0.344	0.424	0.0019	0.033	8.0

driven by a vibrating structure, as demonstrated in Ref. [13]. Using structural vibrations from a loudspeaker, rather than employing signals of sound pressure variations, offers significant computational resource savings.

Given the considerations mentioned above, the methodology employed to analyze the arching profile of the violin in this study was divided into three steps: 1.- obtaining the Impulse Response (IR) of a parametrically designed violin soundbox, 2.- generating the input force based on how the bowed strings drive the bridge, and 3.- utilizing the data from the previous steps to produce audio files. This approach makes sense as it involves playing structural vibrations from a loudspeaker, thereby avoiding the need for calculating signals of sound pressure variations for faster explorations.

2. Methods

2.1. The real violin

A replica of a Stradivari violin, the Titian 1715, served as the basis for the computational model presented in this paper (see Fig. 1). The overall geometry of this replica was meticulously crafted using traditional techniques, closely following measurements and CT scans of the original Titian, as detailed in Ref. [14]. Prior to this study, finite element simulations were employed to guide the design of the free plates in the replica, aiming to achieve specific resonant frequencies for the second and fifth free modes in both the top and back plates. The simulation results guided the determination of the final thickness of the physical replica. It is noteworthy that accessories of the violin and the neck were not considered in the simulations conducted for this study.

The simulation incorporated orthotropic materials to model the woods, adhering to a standard assumption. Key properties of the spruce and maple used in the physical replica were determined by measuring resonant frequencies in samples extracted from each wood type (refer to Table I). For the remaining properties, existing data from the model in Ref. [11] were employed. Real wood properties were obtained through the extraction of rectangular samples, aligning their longer sides with the long-grain and cross-grain directions of the wood. This alignment allowed for the correlation of their lowest resonances with the elastic properties influencing the corresponding frequencies. The samples were also utilized for measuring wood densities. Further details on this process can be found in a previous paper by the working group [15].

2.2. Adjusting the arching profile

Even when utilizing numerical methods, establishing a procedure to examine the implications of adjusting the arching profiles involves considering various factors. The initial step involved determining the permissible limits for varying the arching height, measured without factoring in the thickness of the plate, within $\pm 10\%$ of the replica's height (refer to Table II). By adjusting the arching profiles within this range, we ensured that geometries representative of real violins could still be obtained. Furthermore, the consequences of altering the arching profiles in the top and back plates were analyzed independently. To investigate variations in the top plate, the bass bar was removed to eliminate any shape changes resulting from its adaptation to different arching profiles.

2.3. Comparing violin behaviors

The data for comparing the vibrational behavior of various violin designs were generated through two distinct methods. The first method followed the conventional approach for analyzing instruments in violin acoustics, utilizing bridge mobility. In this study, bridge mobilities were computed by applying excitation to the bass corner of the bridge in the violin model. The velocity response at the opposite corner was then calculated to derive the IR. Subsequently, these IRs, in the time domain, were organized in a text file formatted as required by AnELyzer. AnELyzer is an open-source application previously developed by the author [16] specifically for calculating bridge mobilities from violin measurements. The referenced paper provides more comprehensive explanations regarding bridge mobility measurements.

Another approach employed to compare the behavior in the models involved the utilization of sound files generated through numerical calculations. To emulate violin vibrations

TABLE II. Maximum height in mm of the arching profile in the plates for the original model and after being applied variations of $\pm 10\%$ for the tests.

plate	original	lower	higher	edge thick
top	12.1	10.9	13.3	3.5
back	13.7	12.3	15	3.5

FIGURE 1. Replica of the 1715 Stradivari's violin "Titian" and the finite element model of its soundbox.

as the sound source, a stereo loudspeaker system was utilized, offering a more meaningful representation than a loudspeaker reproducing the sound pressure at a single point in space (*i.e.*, the signal that a microphone would capture). The left loudspeaker was driven using data corresponding to the Helmholtz-like sound hole resonance, while the vibrations of the right loudspeaker mimicked the vibrations of the violin body, specifically focusing on a node on the island of the violin model. In this manner, several sound files in *.wav* format were created.

3. Finite element model

The finite element model of the violin body utilized in this study was based on the free code published in Ref. [11]. However, this version was significantly enhanced by incorporating at least three new features:

1. Individual Damping Control: The ability to impose individual damping on selected modes of interest was introduced.

2. Improved Transient Analysis: The time required for computing transient analysis was significantly reduced by implementing the mode superposition analysis detailed in Subsec. 3.3. This approach, as opposed to full transient analysis (refer to [17] for theoretical details), resulted in a considerable decrease in computation time.

3. Enhanced Vibrations Export: Perhaps the most notable addition is the capability to export vibrations of the model. These exported vibrations can be further processed using Scilab to generate sound files.

The FE simulation was conducted using ANSYS® Mechanical APDL 2022 R2, which is freely accessible for models containing fewer than 32000 nodes. The models implemented in this study utilized approximately 30300 nodes, ensuring accessibility for interested individuals. This node count was selected to strike a balance, providing sufficient resolution to achieve a clear representation of the violin shape while remaining within the constraints of the free licensing limit. It is worth noting that with a full ANSYS license, the model's resolution could be further enhanced. However, such access would be subject to significant restrictions for many users.

The instructions necessary for sculpting the model and computing the solutions were formulated parametrically within a single text file. This file, which is freely available upon request, empowers interested individuals to replicate the findings of this study or modify the model by adjusting the parameters designed to control specific features. The entire structure is discretized using approximately 17100 high-order 3-D 10-node elements, identified in ANSYS as SOLID187. This element type exhibits quadratic displacement behavior, making it well-suited for modeling irregular meshes. In the meshing process (depicted in Fig. 1), a maximum element size of 12 mm was enforced.

3.1. Coupling with the enclosed air

In the low-frequency range of the violin, specifically below 650 Hz, optimal model performance necessitates consideration of the two most prominent resonances associated with the enclosed air within the cavity. However, incorporating finite elements to mesh the volume of the enclosed air would result in a model with hundreds of thousands of nodes. Consequently, the computational cost would outweigh the benefits for the primary objective of this work, which is to generate sound using various violin designs. As a pragmatic alternative, an oversimplified representation of the vibratory influence of the air was introduced through the addition of a double mass-spring-damper system to the soundbox. To elucidate the conceptualization of these additions, it is essential to introduce the concept of *component modes*, as employed by Gough [10].

Signature modes are actual vibration modes of the complete violin, and modes, by definition, are not coupled. However, isolated ingredients of the violin as a system exhibit their own modes. Gough called them component modes, since component modes can indeed be coupled, giving rise to the actual, uncoupled, modes of the complete structure. He uses lower case for component modes, and upper case for the actual mode. This nomenclature has been consistently employed throughout the rest of this section for clarity in the explanations.

The first strong resonance involving the enclosed air of the cavity, considered for a good performance of the model, was $A_0 \approx 275$ Hz. It has been successfully explained in the literature using a Helmholtz resonator as a component mode, denoted by a_0, but with a lower frequency caused by the coupling with flexible walls of the soundbox. For typical dimensions of a violin soundbox, the frequency for this component mode is a_0=300 Hz. Consequently, the mass-spring-damper system replacing a_0 was tuned to 300 Hz. This system was attached at the bass bar, as this location experiences maximum deflections of the soundbox coupled with a_0. The stiffness of the spring was determined by specifying the target frequency, and then, estimating the effective mass, which was set to $m_{eff} = 1.5$ g.

The second air resonance considered in the model is a cavity mode characterized by a transverse nodal line dividing the bouts of the soundbox. This specific component mode is denoted by a_1 and is coupled with another mode of the soundbox, b_1^-, leading to their interaction in the B_1^- signature mode. The typical frequency for a_1 is around 499 Hz, and this value was imposed as the resonance frequency for the mass-spring-damper system intended to represent this component mode. Additionally, the effective mass for a_1 was $m_{eff} = 2$ g to ensure proper coupling.

Since strong displacements of b_1^- are located similarly to those in A_0, and both a_0 and a_1 can undergo coupling through the soundbox, the mass-spring-damper system was attached to the mass of the system corresponding to a_0.

3.2. The parametric model

The model was generated through commands written in a batch file, bypassing the use of the Graphical User Interface (GUI) in ANSYS. The fields of these commands can be populated using algebraic parameters rather than specific numerical values. This approach enables the automatic adjustment of model dimensions when a part is modified. Once the algebraic parameters are appropriately linked to construct the model, its geometry can be swiftly adapted. For instance, modifying the arching profile of the plate necessitates adjusting the bridge position and the size of the soundpost. In the current iteration of the batch file, a parameter has been established to govern the height of the arching profile. Varied values for this parameter result in the automatic update of all affected geometries in the violin, eliminating the need for user intervention.

Attempting to adjust the geometry of an already-created finite element model would be nearly impractical. Instead, in this work, the model is created from scratch every time an adjustment is required by the user; in other words, an existing model is not modified. It's important to note that to replicate an exact shape of the real counterpart of the violin -as in [18]- was not a target of this paper.

3.3. Mode-superposition method for impulse response

The IR, represented in terms of structural velocity in the time domain, was essential for generating the sound of each FE model. In the calculation process, the number of operations needed in a full transient analysis is directly proportional to

the number of time steps. Consequently, the use of implicit direct integration, as employed in full transient analysis, is expected to be effective only when a response for a relatively short duration (*i.e.*, not requiring too many time steps) is needed. However, for this paper, the integration for each IR was defined to be carried out over 4096 time steps with a resolution of 44.1 kHz. Thus, in the equilibrium equations

$$\mathbf{M}\ddot{\mathbf{u}} + \mathbf{C}\dot{\mathbf{u}} + \mathbf{K}\mathbf{u} = \mathbf{f}(t), \tag{1}$$

where $\mathbf{M}$ is the mass matrix, $\mathbf{C}$ is the damping matrix, $\mathbf{K}$ is the stiffness matrix, $\ddot{\mathbf{u}}$ is the nodal acceleration vector, $\dot{\mathbf{u}}$ is the nodal velocity vector, $\mathbf{u}$ is the nodal displacement vector, and $\mathbf{f}(t)$ is the load vector; it may be more effective to first transform into a form in which the step-by-step solution is less costly.

One effective approach is the use of the mode superposition method, which proved to be at least fifteen times faster than full transient analysis for the same type of analysis. This method involves solving the eigenvalues and eigenvectors of the system, followed by solving a set of decoupled equilibrium equations, and finally, superposing the response in each eigenvector -these being the free-vibration mode shapes of the finite element assemblage. The selection between mode superposition analysis and direct integration primarily hinges on numerical efficiency. The solutions derived from either method are practically identical, accounting for numerical errors in the time integration schemes employed and round-off errors in the computational system. For a more in-depth understanding of the mode superposition method, additional details can be found in Ref. [17].

In experimental data of the literature, bridge mobilities measurements usually cover frequencies until 5 kHz. Therefore the superposition simulated in this work was designed to cover until this frequency. To reach 5 kHz in the response of the model, 150 modes must be included.

3.4. Modal damping for individual peaks

In real vibrating systems, the dissipative process is the simultaneous result of various mechanisms, making it challenging to accurately identify and model (see [19]). In the implemented model, two forms of damping were concurrently specified: Rayleigh Damping and Mode-Dependent Damping Ratio. Consequently, in the basic equation of motion solved by the structural dynamic analysis [Eq. (1)], the program will construct the damping matrix $\mathbf{C}$ as the sum of all the specified forms.

Slight damping was introduced to $\mathbf{C}$ in terms of the Rayleigh damping. These values were calculated as only proportional to the stiffness matrix in the form

$$\mathbf{C} = \alpha\mathbf{M} + \beta\mathbf{K}, \tag{2}$$

but in many practical structural problems, mass damping may be ignored so $\alpha = 0$. The value assigned for the analysis here performed was $\beta = 1.2 \times 10^{-6}$.

Furthermore, Mode-Dependent Damping Ratio was incorporated into the model, providing the capability to specify distinct damping ratios for different modes of vibration. This represents another advantage of utilizing calculations from the mode-superposition method of solution, as Mode-Dependent Damping Ratio is not available in full transient analysis. This form of damping defines the damping ratios as a function of mode, augmenting the Rayleigh damping value if specified (as is the case).

The process to dampen a specific mode involves identifying its order of appearance (first mode, second mode, and so forth) to assign an appropriate damping value. A dedicated command within the batch file is utilized to perform this task during the creation of the parametric model. Notably, even an entire hill can be damped if the resonances clustered to form it are collectively selected to be damped using the same value. In this study, both the transition hill and bridge hill were damped in this manner.

4. Forcing the bridge to generate sound

The input signal necessary to generate "violin type" musical sounds is the force applied by the bowed strings on the bridge towards the body. In realistic scenarios, these forces can be directly measured using a piezoelectric force sensor positioned under each string, as demonstrated in Ref. [12]. However, for the specific focus of this paper, a simplified simulated input signal was deemed sufficient. This approach ensures the numerical nature of the procedure is maintained throughout the entire process.

In fact, the strings were deliberately excluded from the model. To account for their structural influence on the bridge, out-of-plane displacements at each of the four-string notches were restricted. Figure 2 illustrates these restrictions with four hollow arrows. Additionally, the bridge feet were fixed to the top plate. To drive the violin, an in-plane force was applied at the corner of the bass side of the bridge, aligning with the direction in which the bow drives the strings (as depicted by the force vector in Fig. 2).

The bowing of the string induces the well-known stick-and-slip motion in the bridge. Consequently, this motion imparts a waveform to the violin that essentially resembles a sawtooth pattern-refer to [9, 20] for further details. However, attempting to generate violin sounds using a pure sawtooth signal yielded unsatisfactory results. A more effective approach involves creating a smoother waveform by incorporating a limited number of harmonics, following the principles of Fourier series for a sawtooth. If n represents the total number of harmonics and f denotes the frequency of the sawtooth, the amplitude y in the time domain for such a waveform is given by:

$$y(t) = \sum_{k=1}^{n} \frac{(-1)^k}{-k} \sin(2\pi k f t). \tag{3}$$

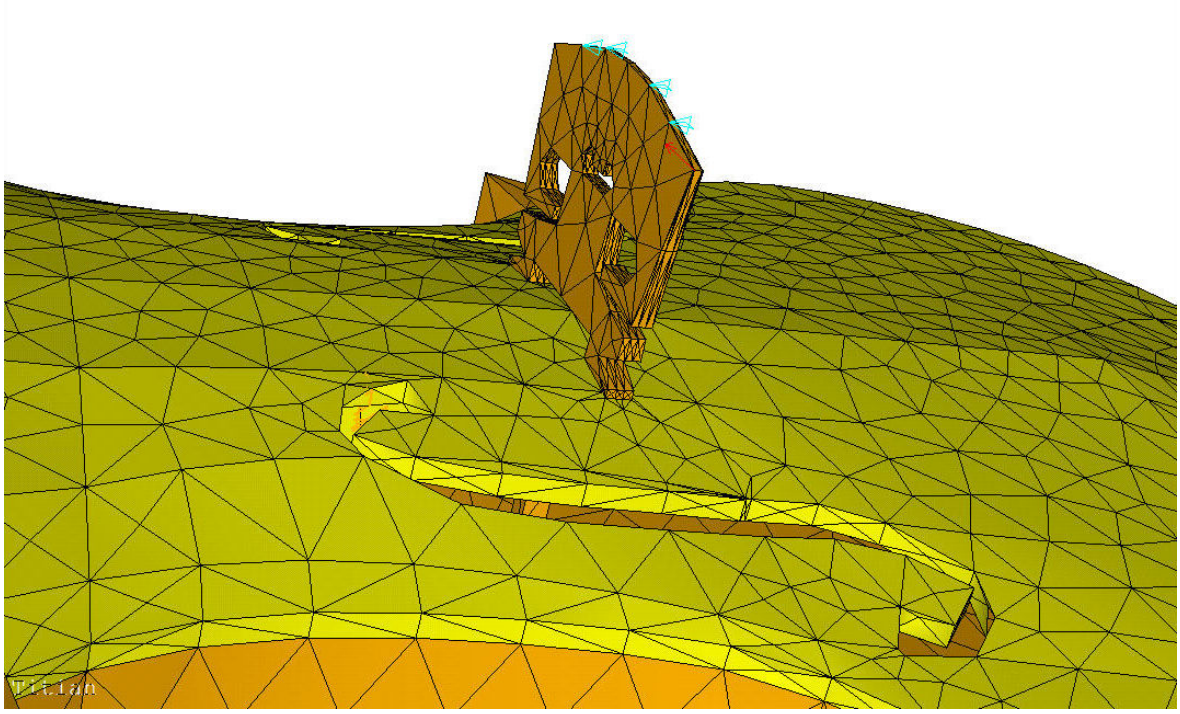

FIGURE 2. The load and constraints of the model. The force vector is shown at the bass corner of the bridge, while the out-of-plane displacements are restricted on the four notches where the strings would be acting.

While the harmonics of a vibrating violin string can extend beyond 10 kHz, the maximum frequency delivered by a bowed string is constrained by the contact area with the bow. This limitation arises because the Helmholtz corner of the vibrating string becomes rounded when passing through the bow-hair ribbon, leading to the suppression of a portion of high-frequency harmonics [9]. For this study, a reasonable proposal for the highest frequency, denoted as f_{cut}, for harmonics generated by Eq. (3) was imposed to be the frequency of the highest mode shape included in the mode superposition method (see Sec. 3.3), namely $f_{\text{cut}} = 5$ kHz. Therefore, the total number of harmonics (Fourier terms) considered to generate the sawtooth was calculated as $n = f_{\text{cut}}/f$.

The initial transient of the bowed string encompasses distinctive features that contribute to the characteristic sound of the violin. It takes a few milliseconds to attain a stable Helmholtz motion, typically around 70 ms. To replicate the inherent instability of a real bowed note during the initial waveforms, the harmonic content in Eq. (3) was deliberately varied from one waveform to another. Let X represent an entire real-valued, continuous random variable within the interval $a \leq X \leq b$, where a and b denote the minimum and maximum number of harmonics in Eq. (3) required to achieve an acceptable performance for $y(t)$. In this manner,

$$y_{\text{instab}}(t) = \begin{cases} y(t) & \text{with} \quad n = X, \quad \text{if } t \leq 70 \text{ ms} \\ y(t) & \text{with} \quad n = a, \quad \text{if } t > 70 \text{ ms} \end{cases}. \tag{4}$$

Furthermore, to capture the characteristic swell in the initial transients of the simulated note governed by Eq. (3), a fade-in effect was incorporated using

$$y_{\text{fade}}(t) = -e^{\gamma t} y_{\text{instab}}(t), \tag{5}$$

where γ represents a negative constant used to regulate the initial amplitude of the signal. In this implementation, $\gamma = -6$ was enforced to achieve a behavior similar to the experimental bowed notes illustrated in Ref. [9]. The subsequent waveforms, constituting the entirety of the note, maintained identical amplitude and harmonic content. Each note, in total, lasted 1.5 seconds. This ensures that when comparing two different files, the test will span the recommended three seconds for subjective evaluations.

Figure 3 depicts some of the initial waveforms after the application of the fade-in (refer to Eq. (5)) and the randomly selected harmonic content, as elucidated in Sec. 4. The alterations in the shape of each waveform are evident, introducing a subtle but audible amount of noise to the original steady-state signal. Both these features were implemented for the initial 100 ms of the audio files [see Eq. (4)] in an attempt to simulate the initial noisy moments of a note bowed on a real violin.

As for the output signal, the IR calculated in terms of velocity through the FE method can be directly routed to the loudspeakers, allowing one to hear how the virtual violins would sound if they were struck on the bridge. Consequently, a stereo audio file was generated for each FE model. To obtain the corresponding signals of the musical notes, it is suf-

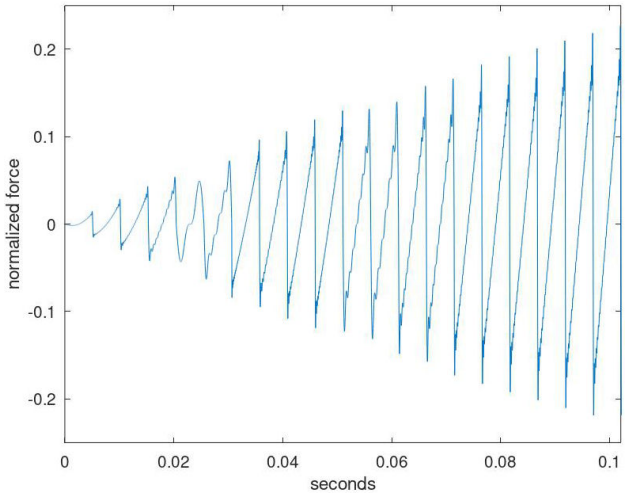

FIGURE 3. Firsts instants of the G note (196 Hz, 26 harmonics) synthesized with the harmonic content randomly varied for each waveform the firsts 70 ms, and applying a fade in.

ficient to convolve the $y_{\text{fade}}(t)$ file with the IR of the system at the node of interest, specifically:

$$\begin{aligned} \text{left channel} &= y_{\text{fade}}(t) * IR_{\text{mass\&spring}} \\ \text{right channel} &= y_{\text{fade}}(t) * IR_{\text{island}}, \end{aligned} \tag{6}$$

where $_{\text{mass\&spring}}$ denotes the node on the mass at the end of the coupled oscillators representing air resonances, $_{\text{island}}$ designates a node located in the area between the f-holes of the violin, and $*$ symbolizes convolution. The convolutions were efficiently executed using Scilab, a robust open-source software for numerical computations, with a single command. Subsequently, the data obtained from the convolution command in Scilab were directly converted into audio files.

5. Results

Prior to utilizing the developed model, a crucial step involved calibration through comparisons with its experimental counterpart. This calibration process specifically focused on the vibrations of the finite element model. Subsequently, the parametric capabilities of the structure were leveraged to conduct an analysis that would be unfeasible using experimental procedures -specifically, the alteration of the arching profile in the top and back plates of the violin. Finally, audio files were generated from models with different arching profiles to assess whether the imposed structural variations could be perceptibly translated into sound.

5.1. Experimental calibration

While the earlier version of the model, as presented in Ref. [11], underwent a robust calibration process, the incorporation of the Mode Damping Ratio in the current version (refer to Subsec. 3.4) notably enhanced the agreement with experimental amplitudes. However, it's crucial to note that

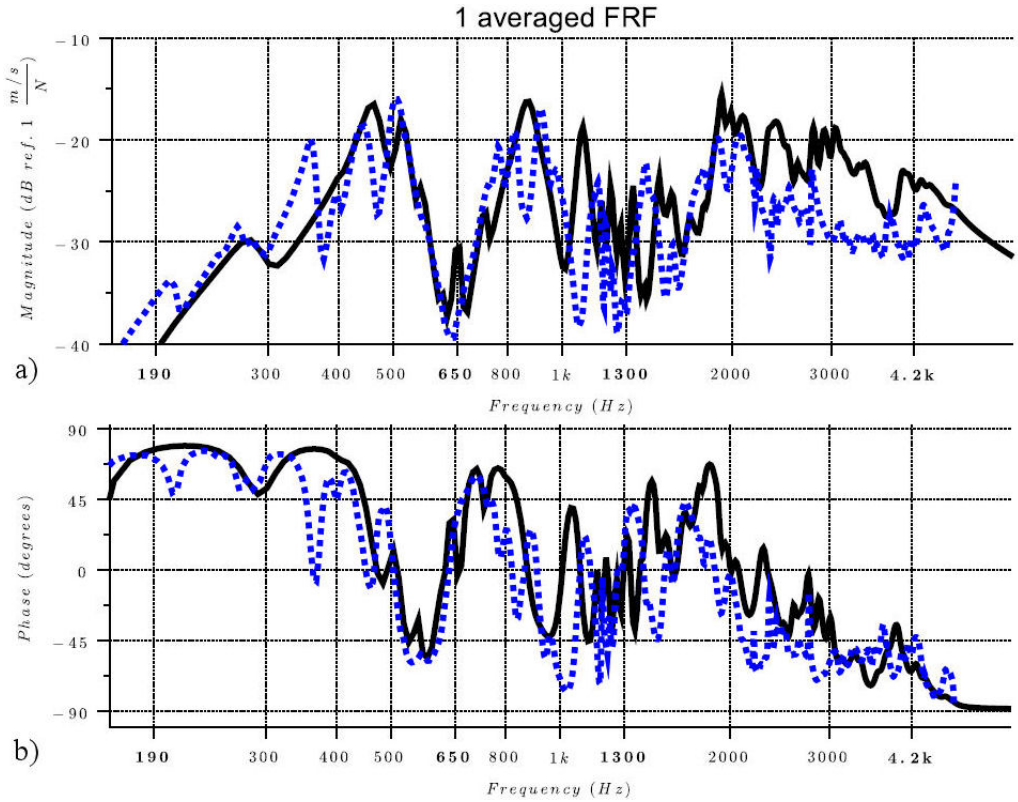

FIGURE 4. Bridge mobility of the Titian replica. The dotted line is the experimental values measured in the real instrument (named Deneb), while the solid line is its corresponding finite element simulation.

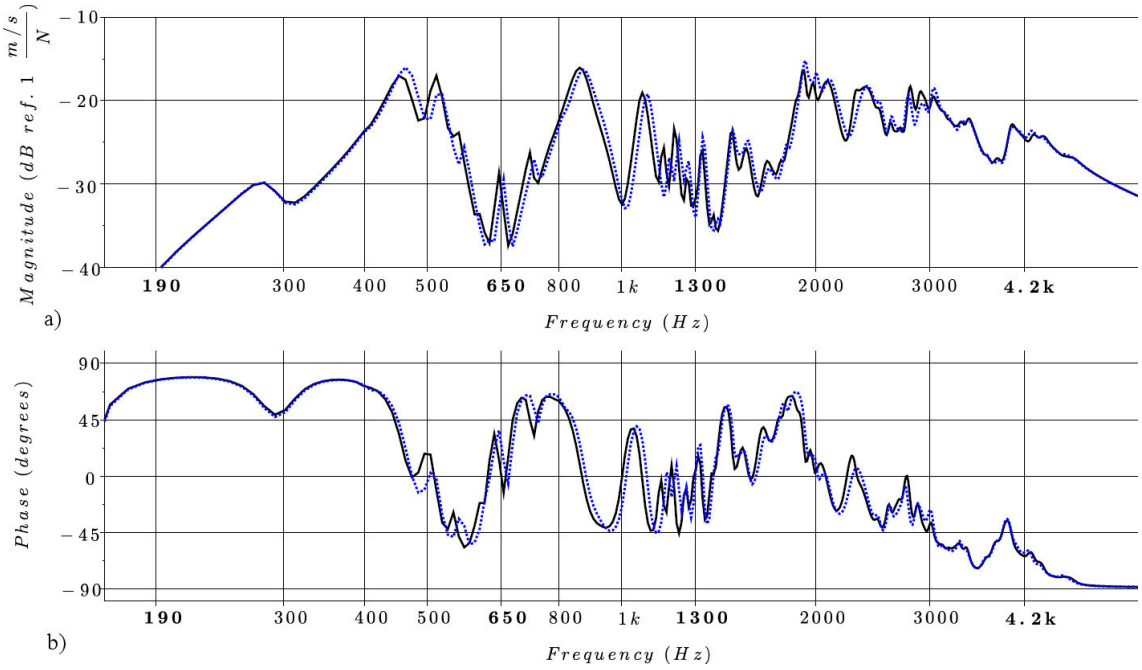

FIGURE 5. Bridge mobilities for two different arching profiles of the back: dotted line is 10% higher than the normal one, while solid line is 10% smaller than the normal.

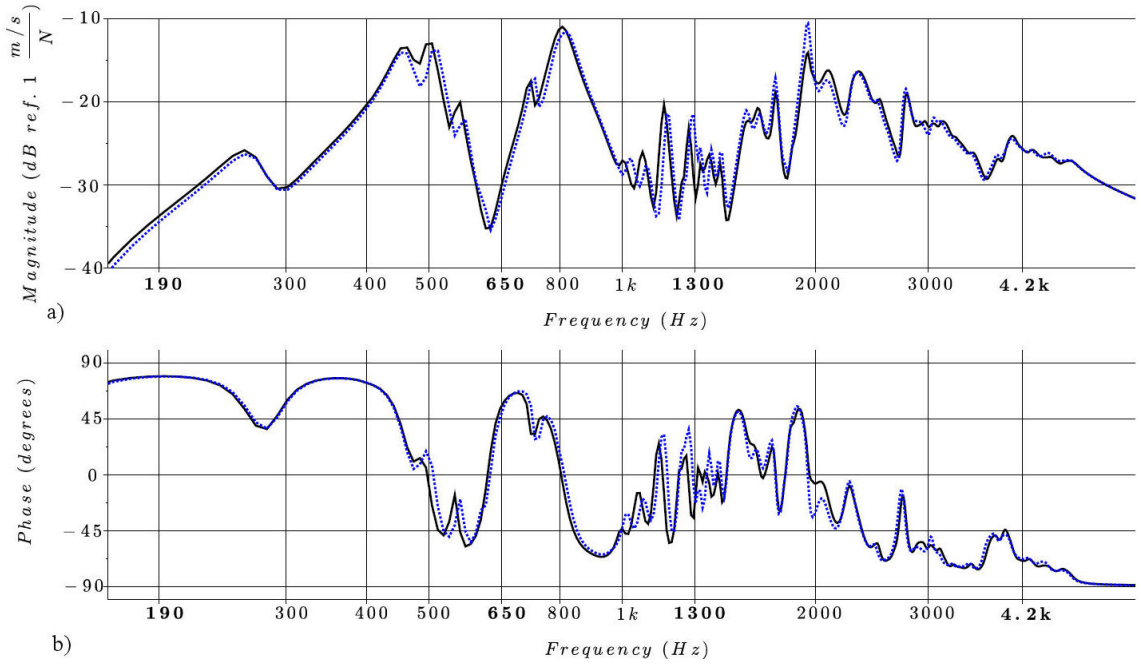

FIGURE 6. Bridge mobilities for two different arching profiles of the top plate: dotted line is 10% higher while solid line is 10% smaller, both compared without including bassbar.

the primary objective was not to achieve a perfect match with data measured on a real violin, but rather to obtain simulated values expected in real violins.

Figure 4 displays the bridge mobilities for both experimental measurements (dotted line) and the model (solid line) based on the same violin. The simulations demonstrate a clear agreement, particularly for the well-separated peaks corresponding to signature modes below 650 Hz, the transition hill spanning 650 Hz to 1300 Hz, and the bridge hill for higher frequencies. The individual damping values determined to align with the experimental data were $A_0 = 0.05$, $B_1^- = 0.03$, $B_1^+ = 0.01$, transient hill $= 0.03$, and bridge hill $= .002$. Notably, this agreement with the behavior of a real violin was achieved even without incorporating strings, accessories, and the neck in the soundbox model.

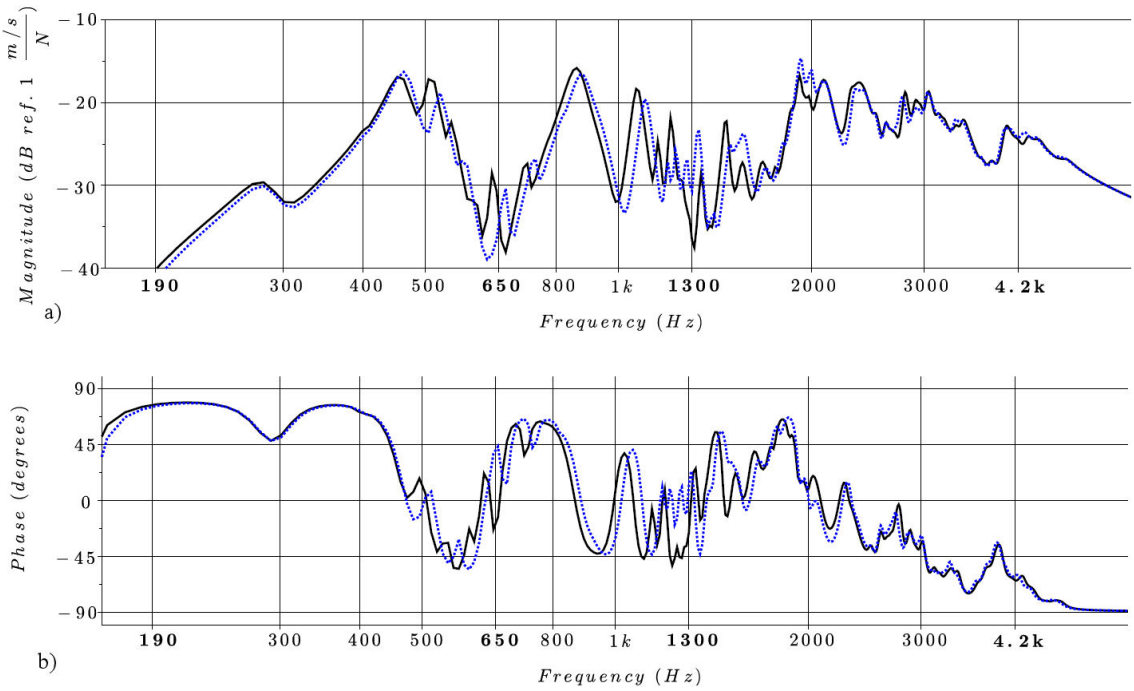

FIGURE 7. Bridge mobilities for two complete soundboxes (including bassbar) varying the arching profiles both in top and back plate: both plates were 10% higher in the dotted line, while solid line is for 10% smaller.

5.2. Adjusting arching profiles

Bridge mobilities, calculated to assess alterations in the arching profile of the plates, were individually plotted for each case. Firstly, Fig. 5 illustrates the corresponding data for the violin model with variations in the arching profile of the back. Subsequently, Fig. 6 depicts the data calculated when only the arching profile of the top plate was varied, with the bassbar removed. This approach was adopted to isolate the changes in the vibrational behavior induced by variations in the top plate, as modifying the height of the arching profile would also impact the shape of the bassbar.

The analysis of the mobilities revealed that, for both plates, augmenting the height of the arching profile resulted in a slight yet discernible overall increase in the modal frequencies of the system. Moreover, the amplitude decreased for peaks between 1.5 kHz and 2 kHz because they are thicker and lower. This effect was more pronounced when altering the arching profile of the top plate.

After analyzing the results presented in Fig. 5 and 6, there was an additional interest in combining the plates to observe the collective impact of similar changes in the response. To address this, two new models were created. In one model, the arching profile in both the top and back plates was increased, while in the other model, the arching profile in both plates was decreased. In both cases, where higher and lower arching profiles were applied, the bassbar was already attached. The bridge mobility of each new model was plotted in Fig. 7, highlighting the differences between the overlapped responses of both models more clearly than in the individual cases of Fig. 5 and 6. Across a broad frequency range, from 500 Hz to 2 kHz, the responses of both models exhibit notable distinctions. Specifically, the frequencies of the peaks are higher in the case of the taller plates. Moreover, when comparing the responses of both models, significant differences in amplitude were observed for the peaks around 1.3 kHz.

5.3. Generating sound files

While the vibratory differences induced by the modification of the arching profile of the plates are evident in the mobility plots, the primary objective of this paper was articulated in obtaining sound from different violin designs. A straightforward approach to compare the performance of each model involved listening to the simulated sound produced by tapping the bridge. However, assessing the sound quality of a violin solely based on tapping the bridge is a non-trivial task. To provide more manageable interpretations, the sound obtained using the input forces calculated for two notes corresponding to open strings of the models, G2 (196 Hz) and D3 (294 Hz), was considered. The audio files created for each model, available by request, are listed below:

TapLowArching.wav Sound obtained by tapping the bass corner on the bridge of the violin with top and back plates with *lower* arching profiles.

TapHighArching.wav Sound obtained by tapping the bass corner on the bridge of the violin with top and back plates with *higher* arching profiles.

GnoteLowArching.wav, DnoteLowArching.wav Musical notes obtained forcing the bass corner of the bridge of the violin with top and back plates with *lower*

arching profiles, with the signal created as described in Sec. 4.

GnoteHighArching.wav, DnoteHighArching.wav Musical notes obtained forcing the bass corner of the bridge of the violin with top and back plates with *higher* arching profiles, with the signal created as described in Sec. 4.

Again, the audio files obtained from the velocity response of the model to the input forces are available by request. In both types of sounds, tapping the bridge and bowing the strings, higher plates resulted in treble sounds, while lower plates were associated with a bass sound. The findings presented in this study contribute to advancing our understanding, beyond empirical comments, that minimal variations in the arching profile lead to significant changes in the sound of a violin. The employed procedure effectively supports this assumption, providing a clearer understanding of the types of changes that can be anticipated by altering the design of the arching profile.

6. Conclusions

The synergy of finite element models, analytical input signals, and time-domain filtering enabled us to conduct vibratory studies that were impractical using experimental methods. In the case presented here, an analysis was conducted to explore the consequences, in terms of vibrations and sound, of varying the arching profiles in a detailed violin soundbox model. One of the notable outcomes was that higher arching profiles led to increased frequencies of several resonances in the model, with these consequences being clearly perceptible in the generated sounds.

What was a better arching profile? It will depend on each musician, so there is no unique answer to this question. Opting for higher arching profiles may yield a violin with a brighter sound, and conversely, lower arching profiles might be preferred for a darker tonal quality. However, it's crucial to note that numerous other factors significantly influence the final behavior of a violin. While exploring each of these factors remains an extensive task, the substantial support provided by all the implemented numerical procedures in this study is undeniable.

It is worth mentioning that the arching of a top plate in violins has a different shape to that in the back, and it would be interesting to know what effect this has. In future work, it would also be of interest to investigate the effect of changing the arching profile. There is some speculation in the literature about the possible importance of rather subtle adjustments to arching shape, but former research at this respect would be useful for a better understanding on how the violin works.

Acknowledgements

The real violin replica, named Deneb, and all the calculations to make it were performed through a grant provided by FONCA-UNAM under the terms of the "Arte, Ciencia y Tecnología 2018" program.

1. J. A. Torres and R. R. Boullosa. Influence of the bridge on the vibrations of the top plate of a classical guitar. *Applied Acoustics*, **70** (2009) 1371.
2. G. Orelli P. *et al.*. Collisions in double string plucked instruments: Physical modelling and sound synthesis of the viola caipira. *Journal of Sound and Vibration*, **443** (2019) 178.
3. J. Woodhouse. The acoustics of a plucked harp string. *Journal of Sound and Vibration* (2022) 116669.
4. E. B. Skrodzka, B. Linde, and A. Krupa. Effect of bass bar tension on modal parameters of a violin's top plate. *Archives of Acoustics*, **39** (2014) 145.
5. L. Fu, C. Fritz, and G. Scavone. Perception of violin soundpost tightness through playing and listening tests. *The Journal of the Acoustical Society of America*, **150** (2021) 540.
6. M. D. Stanciu, F. Dinulică, V. Bucur, V. G. Gliga, S. M. Nastac, and M. Câmpean. Changing the vibrational behavior of the wooden thin arched plates-the maestro violins experimental study case. *Thin-Walled Structures* **174** (2022) 109042.
7. R. Inta, J. Smith, and J. Wolfe. Measurement of the effect on violins of ageing and playing. *Acoustics Australia*, **33** (2005) 1.
8. J. Woodhouse and P. M. Galluzzo. The bowed string as we know it today. *ACTA Acustica united with Acustica*, **90** (2004) 579.
9. K. Guettler. Looking at starting transients and tone coloring of the bowed string. *Proceedings of Frontiers of Research on Speech and Music* (2004).
10. C. E. Gough. A violin shell model: Vibrational modes and acoustics. *J. Acoust. Soc. Am.*, **137** (2015) 1210.
11. J. A. Torres, C. A. Soto, and D. Torres-Torres. Exploring design variations of the titian stradivari violin using a finite element model. *The Journal of the Acoustical Society of America*, **148** (2020) 1496.
12. C. Fritz, I. Cross, B. C. J. Moore, and J. Woodhouse. Perceptual tresholds for detecting modifications applied to the acoustical properties of a violin. *The Journal of the Acoustical Society of America*, **122** (2007) 3640.
13. J. A. Torres and R. R. Boullosa. Radiation efficiency of a guitar top plate linked with edge or corner modes and intercell cancellation. *The Journal of the Acoustical Society of America*, **130** (2011) 546.
14. S. Zygmuntowicz. The strad 3d project: Scientists, musicians, and violinmakers study three classic violins. *The Journal of the Acoustical Society of America*, **127** (2010) 1791.

15. J.A. Torres and D. Torres-Torres. Cambios en la propagación de ondas en una tapa de guitarra debidos al abanico y el puente. *Revista Internacional de Métodos Numéricos para Cálculo y Diseño en Ingeniería*, **31** (2015) 228.

16. J. A. Torres. Open source application for mobility measurements on violins. *Computer Applications in Engineering Education*, **26** (2018) 1111.

17. K. J. Bathe. *Finite element procedures*. Klaus-Jurgen Bathe (2006).

18. J. A. Huber *et al.*. A method for generating finite element models of wood boards from x-ray computed tomography scans. *Computers & Structures*, **260** (2022).

19. M. J. Silva and N. M. Maia. *Modal analysis and testing*. Kluwer Academic Publishers, Netherlands, **1st edition** (1999).

20. D. Thompson. Stick-slip motion due to difference in static and dynamic friction. In *Railway noise and vibration: mechanisms, modelling and means of control*. Elsevier (2008).